VOLUME AND RECURRENCE OF SUBMARINE-FAN-BUILDING TURBIDITY CURRENTS

Zane R. Jobe[1], Nick Howes[2], Brian W. Romans[3], and Jacob A. Covault[4]

[1]Department of Geology and Geological Engineering, Colorado School of Mines, Golden, CO 80401

[2]MathWorks, Natick, MA 01760

[3]Department of Geosciences, Virginia Polytechnic Institute, Blacksburg, VA 24060

[4]Bureau of Economic Geology, Jackson School of Geosciences, The University of Texas at Austin, TX 78758

ABSTRACT

Submarine fans are archives of Earth-surface processes and change, recording information about the turbidity currents that construct and sculpt them. The volume and recurrence of turbidity currents are of great interest for geohazard assessment, source-to-sink modeling, and hydrocarbon reservoir characterization. Yet, such dynamics are poorly constrained. This study integrates data from four Quaternary submarine fans to reconstruct the volume and recurrence of the formative turbidity currents. Calculated event volumes vary over four orders of magnitude (10^5 to 10^9 m^3), whereas recurrence intervals vary less, from 50 to 650 years.

The calculated turbidity-current-event volume magnitudes appear to be related to slope position and basin confinement. Intraslope-fan deposits have small event volumes (~ 10^6 m^3)

while ponded-fan deposits have very large event volumes (10^8 to 10^9 m^3). Deposits in non-ponded, base-of-slope environments have intermediate values (10^7 to 10^8 m^3). Sediment bypass in intraslope settings and flow trapping in ponded basins likely accounts for these differences. There seems to be no clear relationship between event recurrence and basin confinement. Weak scaling exists between event volume and source-area characteristics, but sediment storage in fluvial and/or intraslope transfer zones likely complicates these relationships. The methodology and results are also applied to reconstruct the time of deposition of ancient submarine-fan deposits.

The volume and recurrence of submarine-fan-building turbidity currents form intermediate values between values measured in submarine canyons and channels ($<10^5$ m^3 and $<10^1$ yr) and on abyssal plains ($>10^8$ m^3 and $>10^3$ yr), indicating that small, frequent flows originating in submarine canyons often die out prior to reaching the fan, while rare and very large flows mostly bypass the fan and deposit sediment on the abyssal plain. This partitioning of flow volume and recurrence along the submarine sediment-routing system provides valuable insights for better constraining geohazards, hydrocarbon resources, and the completeness of the stratigraphic record.

INTRODUCTION

Turbidity currents carry sand and mud into the deep sea and create submarine fans, the largest sediment accumulations on Earth (Talling *et al*., 2015). Submarine fans are important depositional archives of climate change (Gulick *et al*., 2015; Bernhardt *et al*., 2017), sea-level fluctuations (Castelltort *et al*., 2017), rates of continental erosion (Clift, 2006), land-to-sea delivery of organic carbon (Burdige, 2005), and continental-margin seismicity (Goldfinger, 2011). They also host significant hydrocarbon resources (Pettingill & Weimer, 2002). Submarine fans exhibit radial or cone-like morphologies in plan view and are composite features, consisting of channel (with or without external levees) and lobe deposits (Shepard & Emery, 1941; Dill *et al*., 1954; Menard, 1955; Heezen *et al*., 1959; Bouma *et al*., 1985). Submarine fans form in net-depositional environments of continental-margin sediment-routing systems, commonly associated with slope breaks that promote sudden deceleration of turbidity currents and localized deposition of sand beyond the slope break (Mutti & Normark, 1987; Adeogba *et al*., 2005; Spinewine *et al*., 2009; Fernandez *et al*., 2014; Jobe *et al*., 2016; Picot *et al*., 2016). The focus of this paper is on the stratigraphic record of submarine fans, as their deposits likely contain a more complete record of turbidity-current volume and recurrence (Piper & Normark, 1983) as compared to channelized elements that are primarily conduits for turbidity-current bypass (Hubbard *et al*., 2014; Stevenson *et al*., 2015).

The volume and recurrence of submarine-fan-building turbidity currents are of interest for the assessment of geohazards, including tsunami hazards (Bondevik *et al*., 1997; Goldfinger, 2011) and damage to submarine infrastructure (Carter *et al*., 2012; Cooper *et al*., 2013), inputs for numerical models of sediment-routing systems (Petit *et al*., 2015; Bolla Pittaluga & Imran, 2014; Sylvester *et al*., 2015), and characterization of subsurface hydrocarbon resources (Saller *et al*., 2008). Studies utilizing outcrops, modern systems, and physical experiments provide insight into the stratigraphic architecture and morphodynamics of submarine channel-fan depositional systems (Normark, 1970; Pirmez *et al*., 1997; Hodgson *et al*., 2006; Sequeiros *et al*., 2010; Hubbard *et al*., 2014; Cartigny *et al*., 2013; de Leeuw *et al*., 2016). Direct monitoring in modern systems provides insight into the short-term morphodynamic and sediment-transport mechanisms (Paull *et al*., 2010; Cooper *et al*., 2013; Hughes-Clarke, 2016; Clare *et al*., 2016). However, understanding the longer-term (>10^2 yr) recurrence of turbidity currents and the stratigraphic evolution of submarine fans remains elusive (Talling *et al*., 2015). In particular, few estimates of sediment volume and recurrence of Holocene fan-building flows have been attempted, and the few calculated volumes to date range seven orders of magnitude, from 10^{-5} to 10^2 km^3 (Piper & Aksu, 1987; Gonzalez-Yajimovich *et al*., 2007; Clare *et al*., 2016). Event recurrence is better constrained, with Quaternary core-based studies providing recurrence interval data from multiple basins (Clare *et al*., 2014, 2016). Studies have also focused on the distribution of event recurrence and how allogenic forcing and position along the sediment-routing system can affect the recurrence distribution (Clare *et al*., 2015; Allin *et al*., 2016, 2017).

This study integrates seismic-reflection and core datasets from Quaternary submarine fans to reconstruct the volume and recurrence of turbidity currents using simple parameters from their deposits. This study focus on the following fans: 1) the Golo fan system, Corsica (Deptuck *et al*., 2008; Sømme *et al*., 2011; Calvès *et al*., 2012), 2) the 'X' intraslope fan, Nigeria (Pirmez *et al*., 2000; Prather *et al*., 2012a; Jobe *et al*., 2016), 3) the Brazos-Trinity intraslope fan system, Texas (Beaubouef & Friedmann, 2000; Mallarino *et al*., 2006; Pirmez *et al*., 2012; Prather *et al*., 2012b), and 4) the Hueneme fan, California (Gorsline, 1996; Normark *et al*., 1998; Romans *et al*., 2009). Using the calculated ranges of event volume and recurrence, we estimate the time of fan deposition in ancient submarine-fan successions, which commonly have poor age-constraints. Finally, we discuss possible linkages between event volume and recurrence with 1) source-area characteristics and 2) basin confinement and slope position.

ESTIMATION OF TURBIDITY CURRENT VOLUME AND RECURRENCE

This study presents a simple formulation that can be used to estimate sediment supply to submarine fans in areas where data are sparse. While more sophisticated sediment mass balance formulations exist (Paola & Voller, 2005 for short-term (sec) bed evolution), such calculations require measurement of sediment concentration and flow velocity, which are very difficult to obtain (Xu *et al*., 2014; Talling *et al*., 2015). The approach utilized here relies on three basic measurements of submarine-fan deposits from seismic-reflection and core data (Fig. 1): 1) total sediment volume V (m^3), (2) total duration of deposition T (yr), and (3) event count n. The sediment volume V of a deposit was determined from seismic-reflection data using thickness of mapped seismic-reflection horizons. When not provided by the original study, the bulk volume was converted to sediment volume using reported porosity values using the equation bulk volume*(1-porosity) = sediment volume. The total duration of deposition T was calculated using chronologic information correlated between core data along seismic-reflection horizons that bound submarine-fan deposits. Finally, the event count n is the number of turbidity-current deposits in the volume V, and was determined from core data (Fig. 1). The event count is simply the number of sand beds present in a core (Fig. 3). Where possible, amalgamated beds are identified (core 'fan 14 3 inch' in Figure 3), but it is possible that some amalgamated beds are unaccounted in the event count n. There is no interpreted hemipelagic sediment in the cores (cf. Talling *et al*., 2007a), and so we assume that the cores are composed entirely of turbidites and do not include appreciable hemipelagic sediment. We also assume that there has been no post-depositional erosion, reworking, or mass wasting. However, we recognize that these processes occur, even in distal parts of submarine fans (Dennielou *et al*., 2017; Croguennec *et al*., 2017). While we appreciate that event-bed geometries in submarine-fan deposits can be more complex (Deptuck *et al*., 2008; Jobe *et al*., 2016), we also assume that core data accurately record the event count n and that all events spread evenly across the fan/lobe. Where possible, an attempt is made to define ranges of V, T, and n from multiple datasets to better encapsulate measurement uncertainty and possible sampling bias from non-uniform deposition and the aforementioned assumptions. Reasoning may suggest to only include the highest value of n as it samples the true event count (Fig. 3), but we conservatively include the range derived from multiple cores where possible because basin setting or other local factors may affect the spatial distribution of events.

The recurrence interval r (yr) is defined as the total time T divided by the event count n (Eq. 1a). Turbidity-current frequency f (yr^{-1}) has the inverse relationship (Eq. 1b):

$r = \frac{T}{n}$ (Eq. 1a); $f = \frac{1}{r}$ (Eq. 1b)

The average sediment volume deposited during a turbidity-current event (v_e) is related to the total volume of a sediment package V (m^3) and the number of events (n):

$v_e = \frac{V}{n}$ (Eq. 2)

These relationships can be combined into an equation that equates the long-term deposition rate and the average event volume and event recurrence (Eq. 3).

$\frac{V}{T} = \frac{v_e}{r} = v_e f$ (Eq. 3)

It is important to note that v_e is an *average* event volume, and does not take into account the distribution of flow volumes shown in natural systems (Talling *et al*., 2007a; Cooper *et al*., 2013; Clare *et al*., 2014; Allin *et al*., 2017) and the spatial distribution of beds on a submarine fan (Deptuck *et al*., 2008; Jobe *et al*., 2016). However, not enough detail about these distributions are available to model them properly. Other assumptions about v_e include: 1) all sediment in an individual turbidity current is deposited on the fan (Lamb *et al*., 2004; Sylvester *et al*., 2015) and no deposition occurs in the canyon-channel system; 2) there is zero bypass to down-system sites; 3) there is no erosional bulking of the flows during transport; 4) there is no temporal change in v_e

during fan/lobe/feeder channel evolution (cf. Deptuck *et al*., 2008; Clare *et al*., 2016). While these assumptions sometimes oversimplify the complexity of submarine-fan depositional systems, they provide a general framework for estimating event volume (v_e) and recurrence (r) for systems with limited data.

STUDY LOCATIONS

This study focuses on late Quaternary (< 130 ka) submarine-fan deposits, which are suitable for determining V, T, and n due to high-quality seismic-reflection data and age-constrained core data. The locales in this study occupy intraslope and base-of-slope settings (Fig. 2, Table 1).

Niger X fan system, Nigeria

Mobile shale deformation of the Niger continental slope (Pirmez *et al*., 2000) created intraslope accommodation where the Niger X submarine fan system was deposited. Jobe *et al*. (2016) described late Quaternary deposits on the X fan and constrained V, T, and n of the youngest sediment package (Fig. 2; Fig. 3; Table 2). The range of V is derived from the deposit area and thickness measurements from cores (Table 2). The range of n is obtained by counting event beds from two core descriptions (Fig. 3). The range of T is provided by adding/subtracting the analytical error from radiocarbon ages to the value provided by Jobe *et al*. (2016). Prather *et al*. (2012a) also measured values of V for longer term (> 100 kyr), thicker (>100 m) deposits on the X fan, but these deposits are not included in our calculations because core data are lacking to constrain T and n.

Hueneme Fan system, California

The Hueneme submarine fan developed in the Santa Monica Basin, offshore California Continental Borderland (Fig. 2). The Quaternary fill of the Hueneme fan is ponded due to faults and folds associated with transpressional deformation related to the San Andreas Fault system (Piper & Normark, 2001; Normark *et al*., 2006). Romans *et al*. (2009) measured *V* for five intervals defined from seismic-reflection profiles that covered the entire Hueneme fan system, and calculated *T* using radiocarbon ages from a core collected by Ocean Drilling Program (Site 1015; Table 2). The five intervals are grouped into three packages (Hueneme 1, 2, and 3-4-5, following nomenclature of Romans *et al*., 2009) that have values of $n > 2$ (for statistical purposes) and approximately equal volume and time duration (Table 2). Ranges of *n* are dependent on including or not including thin silt intervals and debris flow deposits, and minimum and maximum values are presented based on this criterion (Table 2). The youngest package (Hueneme 3-4-5) includes *T* and *n* values estimated by Gorsline (1996) from box cores taken in a more proximal position. While some of the small, frequent flows discussed by Gorsline (1996) may die out prior to reaching the Hueneme fan, these data are included as a conservative approach to defining the parameter space of v_e and *r*.

Brazos-Trinity system, Gulf of Mexico

There are four linked intraslope salt-withdrawal basins in the Brazos-Trinity system that contain Quaternary submarine-fan deposits (Winker, 1996; Badalini *et al*., 2000; Beaubouef & Friedmann, 2000; Mallarino *et al*., 2006). Prather *et al*. (2012b) used 3D seismic-reflection data to map the basin stratigraphy and demonstrate coeval deposition of three packages of sediment in basins II and IV (40 series, 50/60 series, and 70 series in Table 2). Pirmez *et al*. (2012) used borehole and core chronostratigraphy to calculate a sediment budget for the system, estimating *V* and *T* for the three packages. Ranges of *T* were derived from minimum and maximum estimates

(Pirmez *et al*., 2012). Ranges of *n* (Table 2) were derived for each package from the International Ocean Discovery Program Site U1320 core description (fig. 4 of Pirmez *et al*., 2012) in a similar manner to that described for the Hueneme fan (above).

Golo fan system, Corsica

The comparatively small (cf. Sømme *et al*., 2009) Golo submarine-fan deposits can be entirely mapped on seismic-reflection profiles and exhibit base-of-slope fan architecture (Deptuck *et al*., 2008). Values of *V* and *T* were derived from Sømme *et al*. (2011) for Holocene deposits (horizon K to seafloor) and from Calvès *et al*. (2012) for late Quaternary units S1, S2, and S3 and also a Holocene fan package that occupies an intraslope position (the 'Pineto lobe' of Deptuck *et al*., 2008). Values of *n* were derived from two cores in Golo submarine-fan deposits (Gervais, 2002; Gervais *et al*., 2006). The cores used (kco62, kco58 upper section, and kco58 lower section) yield *n* values of 12, 6, and 8, respectively (figs 10 and 14 of Gervais *et al*., 2006). These cores are shallow piston cores and do not penetrate the entire intervals of interest; thus, *n* values for each interval were extrapolated from these core data assuming no temporal change in event recurrence. These extrapolated values of *n* (Table 2) are most appropriate for the youngest deposits, but are also used for the older deposits, acknowledging that there may be temporal changes in event recurrence that are not sampled by existing core data.

DATA ANALYSIS

Using measured values of *V*, *T*, and *n* from each locale, the methodology described above can be used to estimate ranges of event volume and recurrence. Table 2 presents the values of *V*, *T*, and *n* measured from each studied locale. In all four study locales, ranges are often reported for *V*, *T*, and *n* due to measurement uncertainty (e.g., measurement error in ages of Fig. 1) or multiple possible values (Table 2). The Niger X fan is used as an example to explain the measurements and uncertainties of *V*, *T*, and *n*. The sediment volume *V* was calculated using the area of the youngest sediment package and the minimum and maximum thickness measurements of 1 and 3 m based on core penetrations (Fig. 3; Jobe *et al.*, 2016). No areal changes in thickness were assumed, rather a simple area*thickness was used to calculate minimum (1.2 x 10^7 m^3) and maximum (3.6 x 10^7 m^3) values of *V*. The total duration of deposition *T* was determined from core-derived radiocarbon ages (fig. 9 of Jobe *et al.*, 2016) and is estimated to be 4,000 ±200 yr (Fig. 3). The event count *n* was obtained by counting the sand beds in two core descriptions ((*n*=20, *n*=48; Fig. 3; Table 2).

In order to fully explore the parameter space for v_e and *r*, the ranges of the input values *V*, *T*, and *n* are determined by using a uniform distribution (Table 2). To create a uniform distribution of each variable (*V, T, n*), the range between the minimum and maximum values is divided into 10,000 values. Using random sampling with replacement, *r* and v_e are calculated 10,000 times using Equations 1a and 2, respectively. The 10,000 iterations of v_e and *r* for the Niger X fan can be plotted as a ‘size-recurrence’ plot (Fig. 4A).

A triangular distribution is employed which approximates a normal distribution in cases of limited data. For each variable (*V, T, n*), the minimum value, maximum value, and the mean of those two values are used to define the lower limit, upper limit, and peak location of the triangular distribution. Using random sampling with replacement, v_e and *r* are again calculated 10,000 times, with the results displayed in an event volume-recurrence plot (Fig. 4B). A 2D kernel density emphasizes the resulting distribution of v_e and *r*, with the kernel shown as a contour map containing 90% of the data (Fig. 4B). Calculating v_e and *r* from uniform distributions of *V*, *T* and *n* results in the largest, most conservative parameter space (Fig. 4A).

Using a triangular distribution slightly shrinks the overall distribution of the parameter space but does not significantly alter the results obtained with a uniform distribution (Fig. 4B).

RESULTS

For the four studied locales, values of v_e vary over four orders of magnitude (10^5-10^9 m^3), while values of r vary by one order of magnitude (50-650 yr, Fig. 5). The intraslope deposits of the Niger X and Golo Pineto locales show the smallest values of v_e, approximately 10^6 m^3 (Fig. 5). The base-of-slope Golo deposits have intermediate v_e values (10^7 m^3, Fig. 5). The ponded Brazos-Trinity and Hueneme deposits have the largest values of v_e (>10^8 m^3) and the most variability in r (Fig. 5). Interestingly, the three time intervals in the Brazos-Trinity system have quite different values of r but very consistent values of v_e. The Golo Pineto locale has the largest variability in v_e and r of any deposit, likely due to the wide ranges of input values of T and n (Table 2).

Validation of the calculated values of v_e and r

In order to ensure that the calculated values of v_e are reasonable, the distribution of event-bed thickness in a submarine fan deposit can be estimated and compared to well-constrained examples from outcrops and modern systems. For the Niger X fan, values of n (Table 2) and a package thickness of 2 m (the average thickness estimate of Jobe *et al*., 2016) are used to estimate average event-bed thickness of 4.2 cm and 10 cm (for n = 48 and 20, respectively). These thickness values are well within the observed range of event-bed thickness (1-57 cm, average of 10 cm) for cores from the X fan (Jobe *et al*., 2016) as well as other reported event-bed thickness ranges (3-110 cm from Prélat & Hodgson, 2013). These ranges of event-bed thickness are also comparable to other well-characterized submarine-fan deposits (Murray *et al*., 1996; Talling, 2001; Sylvester, 2007; Prélat *et al*., 2009).

DISCUSSION

Estimating the total time of deposition (*T*) in ancient submarine fan deposits

Ancient submarine-fan deposits are well described from subsurface data (Normark, 1970; Saller *et al*., 2008; Kane & Ponten, 2012) and outcrop exposures (Walker, 1978; Hodgson *et al*., 2006; Pyles, 2008; Prélat *et al*., 2009; Auchter *et al*., 2016). Facies relationships and stratigraphic architecture are mappable in outcrops and, with areally extensive exposures, volumes can be estimated. However, the total time of deposition (T) and the event recurrence interval (r) are difficult to determine accurately due to large uncertainties of chronostratigraphic methods for sedimentary rocks. However, we can use estimated volumes (V) for outcropping submarine-fan deposits and calculated ranges of r and v_e from Quaternary systems (Fig. 5) to estimate the total time of deposition T for the ancient, outcropping deposits. These estimates of T can aid in the interpretation of the incomplete and low-resolution geochronology typical of ancient submarine-fan deposits.

Submarine-fan deposits containing six discrete sediment packages were mapped in the Permian Skoorsteenberg Formation in the Tanqua Karoo sub-basin, South Africa by Prélat *et al*. (2009). These six packages were classified hierarchically as ‘lobes’ by Prélat *et al*. (2009) and the encompassing unit a ‘lobe complex’; however, we will refer to them generically as sediment packages to avoid terminology confusion. These submarine-fan deposits are interpreted to have formed in a base-of-slope position in an unconfined (i.e., non-ponded) basin (Prélat *et al*., 2009), most similar to the Golo locale (Table 1). The U-Pb ages from ashes interbedded with the sediment packages of the Skoorsteenberg Formation are all within error of each other (Fildani *et al*., 2009) and may include erroneous ages due to magmatic crustal recycling during volcanic eruptions (McKay *et al*., 2015). Hence, it is not possible to accurately calculate *T* values from these U-Pb ages; it is, however, possible to estimate ranges of *T* using the approach described above. Prélat *et al*. (2009) calculated *V* for three of the mapped packages ('lobes' 2, 5, and 6), with values of 1.3 to 3.5 x 10^9 m^3 (Table 3), similar to calculated sediment volumes from this study (Table 2) and other Quaternary submarine-fan deposits (Prélat *et al*., 2010). Using lobe volume and event count data (Table 2), Equation 2 is used to define potential values of v_e for lobes 2, 5 and 6, which are ~ 10^8 m^3 (Table 2). To be conservative, values of v_e that bracket these estimates are chosen (10^7 to 10^9 m^3), which are also most similar to other base-of-slope systems (Fig. 5). The range of *r* is conservatively chosen as 50-650 yr, encompassing all of the data in Figure 5. Uniform distributions of each variable are created as inputs into Equation 3 (using the same methods as described above) to calculate a range of *T* for the three packages (Fig. 6). The P_{50} prediction of *T* for each package is on the order of 10^4 yr (Fig. 6). Specifically, 'lobe' 2 has T_{P50}=1.5 kyr, 'lobe' 5 has T_{P50}=2.5 kyr, and 'lobe' 6 has T_{P50}=0.9 kyr (Fig. 6). These lobe duration estimates compare reasonably to the Holocene Amazon (15-20 lobes in 10 kyr, Jegou *et al*., 2008) and Zaire (38-52 lobes in 210 kyr, Picot *et al*., 2016) submarine fan deposits (Fig. 6). The hierarchically larger package ('lobe complex' of Prélat *et al*., 2009 often informally referred to as 'Fan 3') consists of six 'lobes'; if minimum and maximum values from Figure 6 are used to estimate *T* for the lobe complex, the range of *T* for 'Fan 3' is 1.6-68 kyr, with median values ranging from 5-15 kyr. This analysis provides a methodology for estimating the total time of deposition (*T*) for ancient submarine-fan successions where no other data are available. This analysis also highlights the need for more volumetric and geochronologic characterization of ancient submarine-fan deposits.

Linking catchment parameters to event volume

Source (e.g., catchment dimensions) and sink (e.g., submarine-fan length) parameters have been shown to generally scale to one another (Sømme *et al*., 2009). The event volume measured in the sink (Fig. 5) should scale to a sediment supply parameter (e.g., sediment load) in the source area, given minimal storage in the transfer zone (Romans *et al*., 2016). In order to investigate these relationships, source parameters (Table 2) were compiled for the four systems from Milliman and Farnsworth (2011), including catchment area (km^2), sediment yield ($tons/km^2/yr$), and sediment load (tons/yr). For the Golo, Hueneme, and Brazos-Trinity systems a weighted average was calculated for catchments that feed these systems (see Table 2), and for the Niger system, one-quarter of the Niger river parameters were used, as Allen (1965) estimates that the study area of the western Niger Delta receives approximately one-quarter of the water and sediment discharge. Figure 7 plots catchment area, sediment yield, and sediment load against the median value of event volume (v_e) calculated for each system, which show positive, but weak, correlations between catchment parameters and event volume. The Niger forms a consistent outlier to this dataset (Fig. 7), suggesting that sediment partitioning in the Niger Delta may not be accurately estimated by Allen (1965); unfortunately, more detailed data are not available. While these scaling relationships (Fig. 7) seem reasonable and corroborate other source-to-sink scaling relationships (Sømme *et al*., 2009), more systems are needed to further test this hypothesis and derive any statistical significance.

The weak scaling shown in Figure 7 indicates poor connectivity between source and sink. When comparing source parameters and event volume, we assume complete transfer of sediment from the source to the sink, but many modern systems have significant sediment storage in the fluvial transfer zone (Wilson & Goodbred, 2015; Romans *et al*., 2016) that could complicate scaling between catchment parameters and v_e. For example, the Niger X system may have significant transfer-zone storage not accounted for by Allen (1965), and thus would plot far below its current position in Fig. **7**.

Linking event volume to the basin setting of submarine fans

While the values of r remain relatively consistent across all basin settings, the values of v_e vary by orders of magnitude (Fig. 5). The studied submarine sediment-routing systems occupy different tectonic and topographic basin settings (Table 1) that may control the values of v_e. (e.g., basin ponding, intraslope basin development). These different basin settings can lead to the sequestration of sediment and thus a further decoupling of the source-to-sink scaling relationships described above. For example, the calculated values of v_e for ponded basin floor settings (the Brazos-Trinity and Hueneme systems) are much larger than for base-of-slope and intraslope fans (Fig. 5). There is no sediment bypass in the Brazos Trinity and Hueneme systems as compared to the intraslope X fan and Golo Pineto locales. The Brazos-Trinity system is fully ponded by a large salt diapir at the distal edge of Basin IV (Prather *et al*., 2012b; Pirmez *et al*., 2012), and the Hueneme fan is ponded by various fault-related ridges and knolls (Normark *et al*., 1998). On the intraslope Niger X fan, on the other hand, there is direct seafloor and core evidence for sediment bypass in the form of an exit channel at the distal edge of the fan (Fig. 3; Jobe *et al*., 2016) and thus small values of v_e may be expected. The Golo Pineto deposit also occupies an intraslope position (Deptuck *et al*., 2008) and likely experienced sediment bypass and thus smaller values of v_e. The larger Golo submarine fan deposits (Fig. 5) occupy a non-ponded base-of-slope position, and thus show intermediate ranges of v_e.

Comparison to other turbidity-current volumes and frequencies: from proximal submarine canyons to abyssal plains

This study focuses on event volumes and frequencies of turbidity currents that build submarine fans. However, there is a full spectrum of event-based measurements from upslope submarine canyons to downslope abyssal plains, measured using direct monitoring data as well as core and outcrop data. These emerging datasets enable a comparison of event volumes and recurrence intervals across the entire submarine sediment-routing system. It is important to note that these trends are only valid for abyssal plains that are fed by the same feeder system as the canyon/channel and fan (cf. Talling *et al*., 2007b).

Abyssal plains

Abyssal plains have been recognized as a source for palaeoclimate (Clare *et al*., 2015) and palaeoearthquake (Goldfinger, 2011) records because they preserve a relatively complete depositional record due to little or no erosion and/or post-depositional modification (Weaver *et al*., 1992). A large compilation by Clare *et al*. (2014) of turbidite volumes (v_e) and recurrence intervals (r) for three abyssal plains allows us to assess the magnitude differences between turbidity currents that build submarine fans and those that deposit sand in the most distal locations on Earth. The data (Clare *et al*., 2014) are derived from well-studied and dated cores from the modern Madeira Abyssal Plain (offshore northwest Africa) and the modern Balearic Abyssal Plain (western Mediterranean Sea), and also from outcrops of the Miocene Marnoso-Arenacea Formation, Italy (Amy & Talling, 2006). Generally, values of v_e and r for turbidity currents building submarine fans are 10-1,000 times smaller and 10-100 times more frequent than turbidity currents depositing sand onto the abyssal plain (Fig. 8). This is an intuitive relationship that was also recognized by Piper and Normark (1983). Large-volume turbidites on abyssal plains can have many triggers, including large-magnitude earthquakes (Normark and Piper, 1991; Piper and Normark, 2011), glacial advances (Haflidason *et al*., 2004), sea-level regressions (Kolla & Perlmutter, 1993), and sea-level transgressions (Hunt *et al*., 2013). However, Clare *et al*. (2014) find that some abyssal plain turbidites are temporally random and not linked to sea level at all. Regardless of the mechanism, abyssal plain turbidites have 10-1,000 times larger event volumes than turbidity currents building submarine fans, but occur 10-100 times less frequently (Fig. 8). However, there is some overlap between the abyssal plain values and large volume flows that characterize the ponded locales of the Hueneme and Brazos-Trinity systems. The ponding in both these systems may result in larger calculated v_e values, as ponding is an effective sediment-trapping mechanism.

Proximal submarine canyons

The heads of submarine canyons, at the other extremity of the submarine sediment routing system, have been instrumented for decades (Prior *et al*., 1987; Paull *et al*., 2010), and have served as natural laboratories that enable a better understanding of turbidity current morphodynamics (Cooper *et al*., 2013; Hughes-Clarke, 2016; Jobe *et al*., 2017; Symons *et al*., 2017). While event volumes have thus far eluded the flow monitoring datasets, recurrence intervals spanning from hours (Hughes-Clarke, 2016) to years (Paull *et al*., 2014) have been documented. However, many of these flows, while very frequent, dissipate prior to reaching the submarine fan (Paull *et al*., 2005; Talling *et al*., 2015) and thus must have relatively small event volumes ($v_e < 10^5$ m^3). Further evidence of frequent and small-volume flows not reaching submarine fans comes from the Iberian abyssal plain (not discussed here, see Allin *et al*., 2017) and the Hueneme submarine fan. Romans *et al*. (2009) suggest that frequent, thin-bedded turbidites with short recurrence intervals (Table 2) recovered in cores from the proximal Hueneme canyon by Gorsline (1996) are not represented in the Hueneme submarine fan deposits, indicating that these frequent, small magnitude flows dissipated prior to reaching the fan.

Event volumes and frequencies across the submarine sediment-routing system

The observations above are summarized in a generalized parameter space for event volume and recurrence (Fig. 8) that is inspired by pioneering work on the size spectrum of turbidity currents (Piper & Normark, 1983). The ranges of event volume and recurrence can be classified into three overlapping categories: submarine canyon, submarine fan, and abyssal plain (Fig. 8). This continuum of flow processes is reflected in the often-smooth geomorphic transition from canyon to fan to basin plain (Piper & Normark, 2001). Small flows are generated in submarine canyons very frequently, but few of those flows reach the submarine fan (Stevens *et al*., 2013; Clare *et al*., 2016). Very large and infrequent flows deposit sediment onto the abyssal plain, and likely partially bypass the submarine fan (Fig. 8). It seems that flows that build submarine fans occupy an intermediate position in terms of event volume (10^5 - 10^9 m^3) and recurrence (10^1 - 10^3 yr), where flow filtering through submarine canyons and channels (McHargue *et al*., 2011) and distance from source (Stevens *et al*., 2013; Allin *et al*., 2017) probably play significant roles in modulating flow volume and recurrence to submarine fans. Thus, fans are constructed by flows large enough to bypass and sculpt canyons, but small enough to die out before reaching the abyssal plain. It is important to note that event volume and recurrence are not single values, but rather distributions, and it is likely that these distributions are truncated as flows move from canyon to basin plain (Allin *et al*., 2017). As more data are collected and analyzed, event volume and recurrence will become better understood and better able to provide sediment flux estimates and assessments of submarine geohazards.

CONCLUSIONS

This study applies a simple mass-balance approach to four well-characterized Quaternary submarine-fan deposits in order to calculate the volumes of sediment deposited by turbidity currents and the recurrence of those events. The ranges of event volume vary over four orders of magnitude, from 10^5 to 10^9 m^3, while recurrence intervals vary by one order of magnitude, from 50 to 650 yr. These flow parameters seem to typify turbidity currents that build submarine fans, and form intermediate values between events measured in submarine canyons and on abyssal plains. Measured turbidity currents in submarine canyons have small volumes (less than 10^5 m^3) and short recurrence intervals (hours to years), while turbidites deposited on abyssal plains have very large event volumes (greater than 10^8 m^3) and long recurrence intervals (10^2 to 10^6 yr). The segmentation of flow volume and recurrence along the submarine sediment-routing system provides valuable insights for better constraining models for geohazard assessment and resource characterization. Calculations of event volume and recurrence can also be used to estimate the time of deposition in ancient submarine-fan successions where high-resolution chronologic data are not available. Applying this methodology, to the well-known 'Fan 3' of the Tanqua Karoo fan system (South Africa), we estimate the time of deposition of Fan 3 to be 5-15 kyr.

The volumes of submarine-fan-building turbidity currents calculated by this study show correlations to slope position and topographic complexity, with ponded submarine fans having larger event volumes than base-of-slope and intraslope fans. Non-ponded intraslope submarine fans have smaller event volumes than ponded or base-of-slope submarine fans, likely because of flow bypass (as opposed to flow trapping in ponded basins) and because only the largest flows reach the basin floor/abyssal plain. There is weak positive scaling of event volume to source area characteristics (e.g., catchment area, sediment yield), but submarine topographic complexity (e.g., ponding, bypass) and sediment storage in the fluvial transfer zone potentially complicate these scaling relationships. Further work should focus on improved volumetric and geochronologic characterization of modern and ancient submarine fan deposits from a range of sediment supply characteristics, source-to-sink configurations, tectonic settings, and geographic locations to enable investigation of trends in event volume and recurrence and how various system characteristics may influence deviations from norms.

ACKNOWLEDGMENTS

We acknowledge reviewers Mike Clare and Joris Eggenhuisen and associate editor Matthieu Cartigny, whose careful and thoughtful reviews greatly enhanced the quality and readability of this article. We also thank Matt Wolinsky, Oriol Falivene, John Martin, Ash Harris, Morgan Sullivan, Hajime Naruse, Zoltan Sylvester, and Alessandro Cantelli for topical discussions. ZRJ acknowledges support from Chevron through the Center of Research Excellence (core.mines.edu), and JAC acknowledges support of the Quantitative Clastics Laboratory sponsors (beg.utexas.edu/qcl).

REFERENCES

Adeogba, A.A., McHargue, T.R. and **Graham, S.A.**, 2005, Transient fan architecture and depositional controls from near-surface 3-D seismic data, Niger Delta continental slope: AAPG Bulletin, v. 89, p. 627–643, doi: 10.1306/11200404025.

Allen, J.R.L., 1965, Late Quaternary Niger delta, and adjacent areas: sedimentary environments and lithofacies: AAPG Bulletin, v. 49, p. 547–600.

Allin, J.R., Hunt, J.E., Talling, P.J., Clare, M.A., Pope, E. and **Masson, D.G.,** 2016, Different frequencies and triggers of canyon filling and flushing events in Nazaré Canyon, offshore Portugal: Marine Geology, v.

371, p. 89–105, doi: 10.1016/j.margeo.2015.11.005.

Allin, J.R., Hunt, J.E., Clare, M.A. and **Talling, P.J.,** 2017, Eustatic sea-level controls on the flushing of a shelf-incising submarine canyon: Geological Society of America Bulletin, v. 130, p. 222–237, doi: 10.1130/B31658.1.

Amy, L.A. and **Talling, P.J.**, 2006, Anatomy of turbidites and linked debrites based on long distance (120 x 30 km) bed correlation, Marnoso Arenacea Formation, Northern Apennines, Italy: Sedimentology, v. 53, p. 161–212, doi: 10.1111/j.1365-3091.2005.00756.x.

Auchter, N.C., Romans, B.W. and **Hubbard, S.M.,** 2016, Influence of deposit architecture on intrastratal deformation, slope deposits of Tres Pasos Formation, Chile: Sedimentary Geology, v. 341, p. 13-26, doi: 10.1016/j.sedgeo.2016.05.005.

Badalini, G., Kneller, B. and **Winker, C.D.,** 2000. Architecture and processes in the late Pleistocene Brazos-Trinity turbidite system, Gulf of Mexico continental slope. In: Weimer, P., Slatt, R.M., Coleman, J., Rosen, N.C., Nelson, H., Bouma, A.H., Styzen, M.J., Lawrence, D.T. (Eds.), Deep-water Reservoirs of the World. Proceedings of the 20th Annual Research Conference. Gulf Coast Section SEPM Foundation, p. 16-34.

Beaubouef, R.T. and **Friedmann, S.J.,** 2000, High resolution seismic/sequence stratigraphic framework for the evolution of Pleistocene intra slope basins, western Gulf of Mexico: depositional models and … (N. C. Rosen, P. Weimer, S. M. Coutes dos Anjos, S. Henrickson, E. Marques, M. Mayall, R. Fillon, T. D'Agostino, A. Saller, K. Campion, T. Huang, R. Sarg, & F. Schroeder, Eds.): Deep-Water Reservoirs of the World,, doi: 10.5724/gcs.12.32.

Bernhardt, A., Schwanghart, W., Hebbeln, D., Stuut, J.-B.W. and **Strecker, M.R.,** 2017, Immediate propagation of deglacial environmental change to deep-marine turbidite systems along the Chile convergent margin: Earth and Planetary Science Letters, v. 473, p. 190–204, doi: 10.1016/j.epsl.2017.05.017.

Bolla Pittaluga, M. and **Imran, J.,** 2014, A simple model for vertical profiles of velocity and suspended sediment concentration in straight and curved submarine channels: Journal of Geophysical Research, v. 119, p. 483–503, doi: 10.1002/(ISSN)2169-9011.

Bondevik, S., Svendsen, J.I., Johnsen, G., Mangerud, J. and **Kaland, P.E.,** 1997, The Storegga tsunami along the Norwegian coast: Its age and run-up: Boreas, v. 26, p. 29–53, doi:10.1111/j.1502-3885.1997.tb00649.x.

Bouma, A.H., Normark, W.R. and **Barnes, N.E.,** 1985, Submarine Fans and Related Turbidite Systems: New York, Springer-Verlag, 351 p.

Burdige, D.J., 2005, Burial of terrestrial organic matter in marine sediments: A re-assessment: Global

Biogeochemical Cycles, v. 19, GB4011, p. 1-7, doi: 10.1029/2004GB002368.

Calvès, G., Toucanne, S., Jouet, G., Charrier, S., Thereau, E., Etoubleau, J., Marsset, T., Droz, L., Bez, M., Abreu, V., Jorry, S., Mulder, T. and **Lericolais, G.,** 2012, Inferring denudation variations from the sediment record; an example of the last glacial cycle record of the Golo Basin and watershed, East Corsica, western Mediterranean sea: Basin Research, v. 25, p. 197–218, doi: 10.1111/j.1365-2117.2012.00556.x.

Carter, L., Milliman, J.D., Talling, P.J., Gavey, R. and **Wynn, R.B.,** 2012, Near-synchronous and delayed initiation of long run-out submarine sediment flows from a record-breaking river flood, offshore Taiwan: Geophysical Research Letters, v. 39, 5 p., doi: 10.1029/2012GL051172.

Cartigny, M.J.B., Eggenhuisen, J.T., Hansen, E.W.M. and **Postma, G.,** 2013, Concentration-Dependent Flow Stratification In Experimental High-Density Turbidity Currents and Their Relevance To Turbidite Facies Models: Journal of Sedimentary Research, v. 83, p. 1046–1064, doi: 10.2110/jsr.2013.71.

Castelltort, S., Honegger, L., Adatte, T., Clark, J.D., Puigdefàbregas, C., Spangenberg, J.E., Dykstra, M.L. and **Fildani, A.,** 2017, Detecting eustatic and tectonic signals with carbon isotopes in deep-marine strata, Eocene Ainsa Basin, Spanish Pyrenees: Geology,, p. G39068.1, doi: 10.1130/G39068.1.

Clare, M.A., Talling, P.J., Challenor, P., Malgesini, G. and **Hunt, J.,** 2014, Distal turbidites reveal a common distribution for large (>0.1 km3) submarine landslide recurrence: Geology, v. 42, p. 263–266, doi: 10.1130/G35160.1.

Clare, M.A., Talling, P.J. and **Hunt, J.E.,** 2015, Implications of reduced turbidity current and landslide activity for the Initial Eocene Thermal Maximum – evidence from two distal, deep-water sites: Earth and Planetary Science Letters, v. 420, p. 102–115, doi: 10.1016/j.epsl.2015.03.022.

Clare, M.A., Clarke, J.E.H., Talling, P.J., Cartigny, M.J.B. and **Pratomo, D.G.,** 2016, Preconditioning and triggering of offshore slope failures and turbidity currents revealed by most detailed monitoring yet at a fjord-head delta: Earth and Planetary Science Letters, v. 450, p. 208–220, doi: 10.1016/j.epsl.2016.06.021.

Clift, P.D., 2006, Controls on the erosion of Cenozoic Asia and the flux of clastic sediment to the ocean: Earth and Planetary Science Letters, v. 241, p. 571–580, doi: 10.1016/j.epsl.2005.11.028.

Cooper, C., Wood, J. and **Andrieux, O.,** 2013, Turbidity current measurements in the Congo Canyon: Offshore Technology Conference OTC-23992-MS, doi:10.4043/23992-MS.

Croguennec, C., Ruffine, L., Dennielou, B., Baudin, F., Caprais, J.-C., Guyader, V., Bayon, G., Brandily, C., Le Bruchec, J., Bollinger, C., Germain, Y., Droz, L., Babonneau, N. and **Rabouille, C.,** 2017, Evidence and age estimation of mass wasting at the distal lobe of the Congo deep-sea fan: Deep-Sea Research Part II,

v. 142, p. 50–63, doi: 10.1016/j.dsr2.2016.12.013.

de Leeuw, J., Eggenhuisen, J.T. and **Cartigny, M.J.B.,** 2016, Morphodynamics of submarine channel inception revealed by new experimental approach: Nature Communications, v. 7, p. 1-7, doi: 10.1038/ncomms10886.

Dennielou, B., Droz, L., Babonneau, N., Jacq, C., Bonnel, C., Picot, M., Le Saout, M., Saout, Y., Bez, M., Savoye, B., Olu, K. and **Rabouille, C.,** 2017, Morphology, structure, composition and build-up processes of the active channel-mouth lobe complex of the Congo deep-sea fan with inputs from remotely operated underwater vehicle (ROV) multibeam and video surveys: Deep-Sea Research Part II, v. 142, p. 25–49, doi: 10.1016/j.dsr2.2017.03.010.

Deptuck, M.E., Piper, D.J.W., Savoye, B. and **Gervais, A.,** 2008, Dimensions and architecture of late Pleistocene submarine lobes off the northern margin of East Corsica: Sedimentology, v. 55, p. 869–898, doi: 10.1111/j.1365-3091.2007.00926.x.

Dill, R.F., Dietz, R.S. and **Stewart, H.,** 1954, Deep-Sea Channels and Delta of the Monterey Submarine Canyon: Geological Society of America Bulletin, v. 65, p. 191–194, doi: 10.1130/0016-7606(1954)65[191:DCADOT]2.0.CO;2.

Fernandez, R.L., Cantelli, A., Pirmez, C., Sequeiros, O. and **Parker, G.,** 2014, Growth Patterns of Subaqueous Depositional Channel Lobe Systems Developed Over A Basement With A Downdip Break In Slope: Laboratory Experiments: Journal of Sedimentary Research, v. 84, p. 168–182, doi: 10.2110/jsr.2014.10.

Fildani, A., Weislogel, A., Drinkwater, N.J., McHargue, T., Tankard, A., Wooden, J., Hodgson, D. and **Flint, S.,** 2009, U-Pb zircon ages from the southwestern Karoo Basin, South Africa--Implications for the Permian-Triassic boundary: Geology, v. 37, p. 719–722, doi: 10.1130/G25685A.1.

Gervais, A., 2002, Analyse multi-échelles de la morphologie, de la géométrie et de l'architecture d'un système turbiditique sableux profond (Système du Golo, Marge est Corse, Mer Méditerranée). Ph.D. Thesis, University of Bordeaux I, no. 2621.

Gervais, A., Mulder, T., Savoye, B. and **Gonthier, E.,** 2006, Sediment distribution and evolution of sedimentary processes in a small sandy turbidite system (Golo system, Mediterranean Sea): implications for various geometries based on core framework: Geo-Marine Letters, v. 26, p. 373–395, doi: 10.1007/s00367-006-0045-z.

Goldfinger, C., 2011, Submarine Paleoseismology Based on Turbidite Records: Annual Review of Marine Science, v. 3, p. 35–66, doi: 10.1146/annurev-marine-120709-142852.

Gonzalez-Yajimovich, O.E., Gorsline, D.S. and **Douglas, R.G.,** 2007, Frequency and sources of basin floor turbidites in Alfonso basin, Gulf of California, Mexico: Products of slope failures: Sedimentary Geology, v. 199, p. 91–105, doi: 10.1016/j.sedgeo.2005.09.025.

Gorsline, D.S., 1996, Depositional events in Santa Monica Basin, California Borderland, over the past five centuries: Sedimentary Geology, v. 104, p. 73–88.

Gulick, S.P.S., Jaeger, J.M., Mix, A.C., Asahi, H., Bahlburg, H., Belanger, C.L., Berbel, G.B.B., Childress, L., Cowan, E., Drab, L., Forwick, M., Fukumura, A., Ge, S., Gupta, S., *et al*., 2015, Mid-Pleistocene climate transition drives net mass loss from rapidly uplifting St. Elias Mountains, Alaska: Proceedings of the National Academy of Sciences, v. 112, p. 15042–15047, doi: 10.1073/pnas.1512549112.

Haflidason, H., Sejrup, H.P., Nygård, A., Mienert, J., Bryn, P., Lien, R., Forsberg, C.F., Berg, K. and **Masson, D.,** 2004, The Storegga Slide: architecture, geometry and slide development: Marine Geology, v. 213, p. 201–234, doi: 10.1016/j.margeo.2004.10.007.

Heezen, B.C., Tharp, M. and **Ewing, M.,** 1959, The Floors of the Oceans I. The North Atlantic, *In* Heezen, B.C., Tharp, M., and Ewing, M. eds., The Floors of the Oceans: I. The North Atlantic, Geological Society of America Special Paper 65, doi: 10.1130/SPE65-p1.

Hodgson, D.M., Flint, S.S., Hodgetts, D., Drinkwater, N.J., Johannessen, E.P. and **Luthi, S.M.,** 2006, Stratigraphic Evolution of Fine-Grained Submarine Fan Systems, Tanqua Depocenter, Karoo Basin, South Africa: Journal of Sedimentary Research, v. 76, p. 20–40, doi: 10.2110/jsr.2006.03.

Hubbard, S.M., Covault, J.A., Fildani, A. and **Romans, B.W.,** 2014, Sediment transfer and deposition in slope channels: Deciphering the record of enigmatic deep-sea processes from outcrop: Geological Society of America Bulletin, v. 126, p. 857–871, doi: 10.1130/B30996.1.

Hughes-Clarke, J.E., 2016, First wide-angle view of channelized turbidity currents links migrating cyclic steps to flow characteristics: Nature Communications, v. 7, p. 1–13, doi: 10.1038/ncomms11896.

Hunt, J.E., Wynn, R.B., Talling, P.J. and **Masson, D.G.,** 2013, Frequency and timing of landslide-triggered turbidity currents within the Agadir Basin, offshore NW Africa: Are there associations with climate change, sea level change and slope sedimentation rates?: Marine Geology, v. 346, p. 274–291, doi: 10.1016/j.margeo.2013.09.004.

Jegou, I., Savoye, B., Pirmez, C. and **Droz, L.,** 2008, Channel-mouth lobe complex of the recent Amazon Fan: The missing piece: Marine Geology, v. 252, p. 62–77, doi: 10.1016/j.margeo.2008.03.004.

Jobe, Z.R., Sylvester, Z., Howes, N., Pirmez, C., Parker, A., Cantelli, A., Smith, R., Wolinsky, M.A., O'Byrne, C., Slowey, N. and **Prather, B.,** 2016, High-resolution, millennial-scale patterns of bed compensation on a sand-rich intraslope submarine fan, western Niger Delta slope: Geological Society of America Bulletin, v. 129, p. 23–37, doi: 10.1130/B31440.1.

Jobe, Z.R., Sylvester, Z., Bolla Pittaluga, M., Frascati, A., Pirmez, C., Minisini, D., Howes, N. and **Cantelli, A.,** 2017, Facies architecture of submarine channel deposits on the western Niger Delta slope: Implications for grain-size and density stratification in turbidity currents: Journal of Geophysical Research: Earth Surface, v. 122, p. 473–491, doi: 10.1002/2016JF003903.

Kane, I.A. and **Ponten, A.S.M.,** 2012, Submarine transitional flow deposits in the Paleogene Gulf of Mexico: Geology, v. 40, p. 1119–1122, doi: 10.1130/G33410.1.

Kolla, V. and **Perlmutter, M.A.,** 1993, Timing of Turbidite Sedimentation on the Mississippi Fan: AAPG Bulletin, v. 77, p. 1129–1141.

Lamb, M.P., Hickson, T., Marr, J.G., Sheets, B. and **Paola, C.,** 2004, Surging versus continuous turbidity currents: flow dynamics and deposits in an experimental intraslope minibasin: Journal of Sedimentary Research, v. 74, p. 148–155.

Mallarino, G., Beaubouef, R.T., Droxler, A.W., Abreu, V. and **Labeyrie, L.,** 2006, Sea level influence on the nature and timing of a minibasin sedimentary fill (northwestern slope of the Gulf of Mexico): AAPG Bulletin, v. 90, p. 1089–1119, doi: 10.1306/02210605058.

McHargue, T., Pyrcz, M.J., Sullivan, M.D., Clark, J.D., Fildani, A., Romans, B.W., Covault, J.A., Levy, M., Posamentier, H.W. and **Drinkwater, N.J.,** 2011, Architecture of turbidite channel systems on the continental slope: Patterns and predictions: Marine and Petroleum Geology, v. 28, p. 728–743, doi: 10.1016/j.marpetgeo.2010.07.008.

McKay, M.P., Weislogel, A.L., Fildani, A., Brunt, R.L., Hodgson, D.M. and **Flint, S.S.,** 2015, U-PB zircon tuff geochronology from the Karoo Basin, South Africa: implications of zircon recycling on stratigraphic age controls: International geology review, v. 57, p. 393–410, doi: 10.1080/00206814.2015.1008592.

Menard, H.W., 1955, Matching Land and Sea Floor Topography and Structures off California: AAPG Bulletin, v. 39, p. 137–137.

Milliman, J.D. and **Farnsworth, K.L.,** 2011, River Discharge to the Coastal Ocean: A Global Synthesis. Cambridge University Press, Cambridge, 384 p.

Murray, C.J., Lowe, D.R. and **Graham, S.A.,** 1996, Statistical analysis of bed-thickness patterns in a turbidite section from the Great Valley Sequence, Cache Creek, Northern California: Journal of Sedimentary Research, v. 66, p. 900–908.

Mutti, E. and **Normark, W.R.,** 1987, Comparing Examples of Modern and Ancient Turbidite Systems: Problems and Concepts, in Marine Clastic Sedimentology, Dordrecht, Springer, Dordrecht, p. 1–38.

Normark, W.R., 1970, Growth Patterns of Deep-Sea Fans: AAPG Bulletin, v. 54, p. 2170–2195.

Normark, W.R., and Piper, D.J.W., 1991, Initiation processes and flow evolution of turbidity currents: implications for the depositional record. SEPM Special Publication no. 46 "From Shoreline to Abyss", p. 207-230.

Normark, W.R., Piper, D. and **Hiscott, R.N.,** 1998, Sea level controls on the textural characteristics and depositional architecture of the Hueneme and associated submarine fan systems, Santa Monica Basin, California: Sedimentology, v. 45, p. 53–70.

Normark, W.R., Piper, D.J.W. and **Sliter, R.,** 2006, Sea-level and tectonic control of middle to late Pleistocene turbidite systems in Santa Monica Basin, offshore California: Sedimentology, v. 53, p. 867–897, doi: 10.1111/j.1365-3091.2006.00797.x.

Paola, C. and **Voller, V.R.,** 2005, A generalized Exner equation for sediment mass balance, J. Geophys. Res., v. 110, F04014, doi:10.1029/2004JF000274.

Paull, C.K., Mitts, P., Ussler, W., Keaten, R., and **Greene, H.G.,** 2005, Trail of sand in upper Monterey Canyon: Offshore California: Geological Society of America Bulletin, v. 117, p. 1134, doi: 10.1130/B25390.1.

Paull, C.K., Ussler, W., III, Caress, D.W., Lundsten, E., Covault, J.A., Maier, K.L., Xu, J. and **Augenstein, S.,** 2010, Origins of large crescent-shaped bedforms within the axial channel of Monterey Canyon, offshore California: Geosphere, v. 6, p. 755–774, doi: 10.1130/GES00527.1.

Paull, C.K., McGann, M., Sumner, E.J., Barnes, P.M., Lundsten, E.M., Anderson, K., Gwiazda, R., Edwards, B. and **Caress, D.W.,** 2014, Sub-decadal turbidite frequency during the early Holocene: Eel Fan, offshore northern California: Geology, v. 42, p. 855–858, doi: 10.1130/G35768.1.

Petit, C., Migeon, S. and **Coste, M.,** 2015, Numerical models of continental and submarine erosion: application to the northern Ligurian Margin (Southern Alps, France/Italy): Earth Surface Processes and Landforms, v. 40, p. 681–695, doi: 10.1002/esp.3685.

Pettingill, H.S. and **Weimer, P.,** 2002, Worldwide deepwater exploration and production: Past, present, and future: The Leading Edge, v. 21, p. 371–376, doi: 10.1190/1.1471600.

Picot, M., Droz, L., Marsset, T., Dennielou, B. and **Bez, M.,** 2016, Controls on turbidite sedimentation: Insights from a quantitative approach of submarine channel and lobe architecture (Late Quaternary Congo Fan): Marine and Petroleum Geology, v. 72, p. 423–446, doi: 10.1016/j.marpetgeo.2016.02.004.

Piper, D. and **Aksu, A.E.,** 1987, The Source and Origin of the 1929 Grand Banks Turbidity Current Inferred from Sediment Budgets: Geo-Marine Letters, v. 7, p. 177–182, doi: 10.1007/BF02242769.

Piper, D. and **Normark, W.R.,** 1983, Turbidite Depositional Patterns and Flow Characteristics, Navy Submarine Fan, California Borderland: Sedimentology, v. 30, p. 681–694, doi: 10.1111/j.1365-3091.1983.tb00702.x.

Piper, D. and **Normark, W.R.,** 2001, Sandy fans--from Amazon to Hueneme and beyond: AAPG Bulletin, v. 85, p. 1407–1438.

Piper, D.J.W., and **Normark, W.R.,** 2009, Processes That Initiate Turbidity Currents and Their Influence on Turbidites: A Marine Geology Perspective: Journal of Sedimentary Research, v. 79, p. 347–362, doi: 10.2110/jsr.2009.046.

Pirmez, C., Hiscott, R.N. and **Kronen, J.,** 1997, Sandy turbidite successions at the base of channel-levee systems on the Amazon Fan: unraveling the facies architecture of large submarine fans: Proceedings of the Ocean Drilling Program. Scientific Results, vol. 155, p. 7-33.

Pirmez, C., Beaubouef, R.T., Friedmann, S.J. and **Mohrig, D.C.,** 2000, Equilibrium profile and base level in submarine channels: examples from Late Pleistocene systems and implications for the architecture of deepwater reservoirs: in Gulf Coast Section SEPM Foundation 20th Annual Bob F. Perkins Research Conference, Global Deep-Water Reservoirs, p. 782-805, doi: 10.5724/gcs.12.32.

Pirmez, C., Prather, B.E., Mallarino, G. and **O'Hayer, W.W.,** 2012, Chronostratigraphy of the Brazos–Trinity depositional System, Western Gulf of Mexico: implications for deepwater depositional models: Application of the Principles ….

Prather, B.E., Pirmez, C. and **Winker, C.D.,** 2012b Stratigraphy of linked intraslope basins: Brazos–Trinity system western Gulf of Mexico: *in* Prather, B.E., Deptuck, M.E., Mohrig, D., van Hoorn, B., and Wynn, R., eds., Application of the Principles of Seismic Geomorphology to Continental-Slope and Base-of-Slope Systems: Case Studies from Seafloor and Near-Seafloor Analogues: Society for Sedimentary Geology (SEPM) Special Publication 99, p. 83-109.

Prather, B.E., Pirmez, C., Sylvester, Z. and **Prather, D.S.,** 2012a Stratigraphic response to evolving geomorphology in a submarine apron perched on the upper Niger Delta slope: *in* Prather, B.E., Deptuck, M.E., Mohrig, D., van Hoorn, B., and Wynn, R., eds., Application of the Principles of Seismic Geomorphology to Continental-Slope and Base-of-Slope Systems: Case Studies from Seafloor and Near-Seafloor Analogues: Society for Sedimentary Geology (SEPM) Special Publication 99, p. 347-369.

Prélat, A. and **Hodgson, D.M.,** 2013, The full range of turbidite bed thickness patterns in submarine lobes: controls and implications: Journal of the Geological Society, v. 170, p. 209–214, doi: 10.1144/jgs2012-056.

Prélat, A., Hodgson, D.M. and **Flint, S.S.,** 2009, Evolution, architecture and hierarchy of distributary deep-water deposits: a high-resolution outcrop investigation from the Permian Karoo Basin, South Africa: Sedimentology, v. 56, p. 2132–2154, doi: 10.1111/j.1365-3091.2009.01073.x.

Prélat, A., Covault, J.A., Hodgson, D.M., Fildani, A. and **Flint, S.S.,** 2010, Intrinsic controls on the range of volumes, morphologies, and dimensions of submarine lobes: Sedimentary Geology, v. 232, p. 66–76, doi: 10.1016/j.sedgeo.2010.09.010.

Prior, D.B., Bornhold, B.D., Wiseman, W.J. and **Lowe, D.R.,** 1987, Turbidity Current Activity in a British Columbia Fjord: Science, v. 237, p. 1330–1333, doi: 10.1126/science.237.4820.1330.

Pyles, D.R., 2008, Multiscale stratigraphic analysis of a structurally confined submarine fan: Carboniferous Ross Sandstone, Ireland: AAPG Bulletin, v. 92, p. 557–587, doi: 10.1306/01110807042.

Romans, B.W., Normark, W.R., McGann, M.M., Covault, J.A. and **Graham, S.A.,** 2009, Coarse-grained sediment delivery and distribution in the Holocene Santa Monica Basin, California: Implications for evaluating source-to-sink flux at millennial time scales: Geological Society of America Bulletin, v. 121, p. 1394–1408, doi: 10.1130/B26393.1.

Romans, B.W., Castelltort, S., Covault, J.A., Fildani, A. and **Walsh, J.P.,** 2016, Environmental signal propagation in sedimentary systems across timescales: Earth Science Reviews, v. 153, p. 7–29, doi: 10.1016/j.earscirev.2015.07.012.

Saller, A., Werner, K., Sugiaman, F., Cebastiant, A., May, R., Glenn, D. and **Barker, C.,** 2008, Characteristics of Pleistocene deep-water fan lobes and their application to an upper Miocene reservoir model, offshore East Kalimantan, Indonesia: AAPG Bulletin, v. 92, p. 919–949, doi: 10.1306/03310807110.

Sequeiros, O.E., Spinewine, B. and **Beaubouef, R.T.,** 2010, Characteristics of velocity and excess density profiles of saline underflows and turbidity currents flowing over a mobile bed: Journal of Hydraulic Engineering, v. 10.1061/(ASCE)HY.1943-7900.0000200, p. 412–433, doi: 10.1061/ ASCE HY.1943-7900.0000200.

Shepard, F.P. and **Emery, K.O.,** 1941, Submarine Topography off the California Coast: Canyons and Tectonic Interpretations: Geological Society of America Special Paper 31, doi: 10.1130/SPE31.

Sømme, T.O., Helland-Hansen, W., Martinsen, O.J., and **Thurmond, J.B.,** 2009, Relationships between morphological and sedimentological parameters in source-to-sink systems: a basis for predicting semi-quantitative characteristics in subsurface systems: Basin Research, v. 21, p. 361–387, doi: 10.1111/j.1365-2117.2009.00397.x.

Sømme, T.O., Piper, D.J.W., Deptuck, M.E. and **Helland-Hansen, W.,** 2011, Linking Onshore-Offshore

Sediment Dispersal in the Golo Source-to-Sink System (Corsica, France) During the Late Quaternary: Journal of Sedimentary Research, v. 81, p. 118–137, doi: 10.2110/jsr.2011.11.

Spinewine, B., Sequeiros, O.E., Garcia, M.H., Beaubouef, R.T., Sun, T., Savoye, B. and **Parker, G.,** 2009, Experiments on Wedge-Shaped Deep Sea Sedimentary Deposits in Minibasins and/or on Channel Levees Emplaced by Turbidity Currents. Part II. Morphodynamic Evolution of the Wedge and of the Associated Bedforms: Journal of Sedimentary Research, v. 79, p. 608–628, doi: 10.2110/jsr.2009.065.

Stevens, T., Paull, C.K., Ussler, W., McGann, M., Buylaert, J.P. and **Lundsten, E.,** 2013, The timing of sediment transport down Monterey Submarine Canyon, offshore California: Geological Society of America Bulletin, v. 126, p. 103–121, doi: 10.1130/B30931.1.

Stevenson, C.J., Jackson, C.A.L., Hodgson, D.M., Hubbard, S.M. and **Eggenhuisen, J.T.,** 2015, Deep-Water Sediment Bypass: Journal of Sedimentary Research, v. 85, p. 1058–1081, doi: 10.2110/jsr.2015.63.

Sylvester, Z., 2007, Turbidite bed thickness distributions: methods and pitfalls of analysis and modelling: Sedimentology, v. 54, p. 847–870, doi: 10.1111/j.1365-3091.2007.00863.x.

Sylvester, Z., Cantelli, A. and **Pirmez, C.,** 2015, Stratigraphic evolution of intraslope minibasins: Insights from surface-based model: AAPG Bulletin, v. 99, p. 1099–1129, doi: 10.1306/01081514082.

Symons, W.O., Sumner, E.J., Paull, C.K., Cartigny, M.J.B., Xu, J.P., Maier, K.L., Lorenson, T.D. and **Talling, P.J.,** 2017, A new model for turbidity current behavior based on integration of flow monitoring and precision coring in a submarine canyon: Geology, v. 45, p. 367–370, doi: 10.1130/G38764.1.

Talling, P.J., 2001, On the frequency distribution of turbidite thickness: Sedimentology, v. 48, p. 1297–1329.

Talling, P.J., Amy, L.A. and **Wynn, R.B.,** 2007a, New insight into the evolution of large-volume turbidity currents: comparison of turbidite shape and previous modelling results: Sedimentology, v. 54, p. 737–769, doi: 10.1111/j.1365-3091.2007.00858.x.

Talling, P.J., Wynn, R.B., Masson, D.G., Frenz, M., Cronin, B.T., Schiebel, R., Akhmetzhanov, A.M., Dallmeier-Tiessen, S., Benetti, S., Weaver, P.P.E., Georgiopoulou, A., Zühlsdorff, C. and **Amy, L.A.,** 2007b, Onset of submarine debris flow deposition far from original giant landslide: Nature, v. 450, p. 541–544, doi: 10.1038/nature06313.

Talling, P.J., Allin, J., Armitage, D.A., Arnott, R.W.C., Cartigny, M.J.B., Clare, M.A., Felletti, F., Covault, J.A., Girardclos, S., Hansen, E., Hill, P.R., Hiscott, R.N., Hogg, A.J., Hughes-Clarke, J., Jobe, Z.R., *et al.*, 2015, Key Future Directions for Research On Turbidity Currents and Their Deposits: Journal of Sedimentary Research, v. 85, p. 153–169, doi: 10.2110/jsr.2015.03.

Walker, R.G., 1978, Deep-water sandstone facies and ancient submarine fans: models for exploration for stratigraphic traps: AAPG Bulletin, v. 62, p. 932–966.

Weaver, P., Rothwell, R.G., Ebbing, J., Gunn, D. and **Hunter, P.M.,** 1992, Correlation, Frequency of Emplacement and Source Directions of Megaturbidites on the Madeira Abyssal-Plain: Marine Geology, v. 109, p. 1–20, doi: 10.1016/0025-3227(92)90218-7.

Wilson, C.A. and **Goodbred, S.L., Jr.,** 2015, Construction and Maintenance of the Ganges-Brahmaputra-Meghna Delta: Linking Process, Morphology, and Stratigraphy: Annual Review of Marine Science, v. 7, p. 67–88, doi: 10.1146/annurev-marine-010213-135032.

Winker, C.D., 1996, High-Resolution Seismic Stratigraphy of a Late Pleistocene Submarine Fan Ponded by Salt-Withdrawal Mini-Basins on the Gulf of Mexico Continental Slope. Offshore Technology Conference OTC-8024-MS. doi:10.4043/8024-MS.

Xu, J.P., Sequieros, O.E. and **Noble, M.A.,** 2014, Sediment concentrations, flow conditions, and downstream evolution of two turbidity currents, Monterey Canyon, USA: Deep-Sea Research Part I, v. 89, p. 11–34, doi: 10.1016/j.dsr.2014.04.001.

Study area (refs.)	Tectonic regime	Slope/Basin Position	Water depth (m)	Distance from shelf edge (km)	Age range (ka)
Niger X system, Nigeria (1), (2), (3)	Passive margin with shale tectonics	Intraslope, not ponded	1200	61	25-15
Hueneme system California (4), (5)	Active; Flexural transpressional basin with fault-controlled basin margins	Basin floor and ponded	850	30	7-0
Golo system, Corsica (6), (7), (8)	Active margin with fault-contolled basin topography	Basin floor, not ponded	800	20	57-15 (5); 130-0 (6)
		Instralope, not ponded	800	20	25-18 (6)
Brazos-Trinity system, Gulf of Mexico (9), (10)	Passive margin with salt tectonics and ponded mini-basin formation	Intraslope, ponded	900 (Basin II); 1500 (Basin IV)	40 (Basin II); 75 (Basin IV)	23-15 (all basins)

Table 1. Characteristics of the locales utilized in this study. References cited include: (1) Jobe *et al*. (2016); (2) Milliman and Farnsworth (2011); (3) Allen (1965); (4) Romans *et al*. (2009); (5) Gorsline (1996); (6) Gervais *et al*. (2006); (7) Sømme *et al*. (2011); (8) Calves *et al*. (2012); (9) Pirmez *et al*. (2012); (10) Prather *et al*. (2012b).

Locale		Bulk volume (m^3)	Porosity	Sediment volume V (m^3) (porosity subtracted)	total time T (years)	n (event bed count)	Catchment Area (km2)	Sediment Yield (tons/km2/yr)	Sediment Load (Megatons/yr)
Niger X	data (min; max)	1.72×10^7; 5.16×10^7	0.4	1.20×10^7; 3.61×10^7	3800; 4400	48; 20	5.50×10^5	4.55	2.5
	notes	using area and 1-3 m thickness from (1)	from multi-sensor core logger data (1)	calculated from bulk volume by subtracting porosity	Fig. 9 of (1)	bend 5; fan 14 cores of (1)	These values represent one-fourth of the Niger River values from (2), as one-fourth of sediment discharge is distributed to the X fan area (3)		
Hueneme Interval 1	data (min; max)	4.58×10^9	0.38	2.84×10^9	2700; 2800	7; 9	5420	2712	14.7
	notes	Table 3 of (4)	Page 1399 of (4)	Table 3 of (4)	Table 3 of (4)	Table 2, Fig 3 of (4)	Summed values of Santa Clara River, Ventura River, and Calleguas Creek from (2)		
Hueneme Interval 2	data (min; max)	3.57×10^9	0.38	2.21×10^9	2340; 2440	6; 8			
	notes	Table 3 of (4)	Page 1399 of (4)	Table 3 of (4)	Table 3 of (4)	Table 2, Fig 3 of (4)			
Hueneme Intervals 3,4,5	data (min; max)	6.12×10^9	0.38	3.80×10^9	500; 1760	4; 7			
	notes	Table 3 of (4)	Page 1399 of (4)	Table 3 of (4)	Value from (5); Fig. 3 of (4)	Value from (5); Fig. 3 of (4)			
Golo Sømme	data (min; max)	Bulk volume to sediment volume performed by (7)		4.04×10^9	14000;16000	68; 136	1214 from (8)	2.2 from (2)	0.002 from (2)
	notes			Table 4 (seafloor to K) of (7)	Fig 7 of (7)	extrapolated from core data of (6)			
Golo Pineto	data (min; max)	Bulk volume to sediment volume performed by (8)		3.12×10^7; 3.55×10^7	2444.5; 6222	12; 53			
	notes			Supp. Table 3 of (8)		extrapolated from core data of (6)			
Golo S1	data (min; max)			8.06×10^9; 1.33×10^{10}	68150; 90700	332; 772			
	notes			Supp. Table 3 of (8)		extrapolated from core data of (6)			
Golo S2	data (min; max)			5.89×10^7; 9.66×10^9	22000; 29090	107; 248			
	notes			Supp. Table 3 of (8)		extrapolated from core data of (6)			
Golo S3	data (min; max)			1.06×10^9; 1.91×10^9	15860; 17100	77; 146			
	notes			Supp. Table 3 of (8)		extrapolated from core data of (6)			
Brazos Trinity 70 series	data (min; max)	Bulk volume to sediment volume performed by (9)		2.72×10^9	2000; 3000	10	1.94×10^5	57.99	11.25
	notes			Fig 15 (all basins) of (9)	Table 2 and pg. 129 of (9)	Fig 4 of (9)	Bsummed values of Brazos, Trinity, and Sabine rivers from (2)		
Brazos Trinity 50/60 series	data (min; max)			1.85×10^9	1100; 1500	12			
	notes			Fig 15 (all basins) of (9)	Fig. 15 and pg. 129 of (9)	Fig 4 of (9)			
Brazos Trinity 40 series	data (min; max)			1.52×10^9	2500; 3900	6			
	notes			Fig 15 (all basins) of (9)	Fig. 15 and pg. 129 of (9)	Fig 4 of (9)			

Table 2. Values of *V*, *T*, *n*, and other pertinent data for the four studied locales. See list of citations in Table 1 for data sources.

Skoorsteenberg Formation lobe deposits (Prelat et al., 2009)	Lobe volume *V* (m^3) from Prelat	event count *n* from Fig. 8 of Prelat	v_e (m^3) using Eqn. 2	Range of *r* (yr) from Fig. 5	*Range of* v_e (m^3) from Fig. 5	*T* (P_{10} estimate, yr)	*T* (P_{50} estimate, yr)	*T* (P_{90} estimate, yr)
Lobe 2	2.2×10^9	7	3.1×10^8	50; 650	1.0×10^7; 1.0×10^9	446	1,526	7,260
lobe 5	3.5×10^9	20	1.8×10^8	50; 650	1.0×10^7; 1.0×10^9	745	2,486	11,339
lobe 6	1.3×10^9	12	1.1×10^8	50; 650	1.0×10^7; 1.0×10^9	273	900	4,332

Table 3. Values of parameters used to calculate total time of deposition (*T*) for submarine-fan deposits of the Skoorsteenberg Formation, South Africa.

Fig. 1. Framework for calculating event volume and recurrence interval of submarine-fan-building turbidity currents, using three variables (*V, T, n*) from deposits. *V* = total sediment volume, *T* = total duration of deposition, *n* = event count, *r* = recurrence interval, v_e = event volume. Figure modified after Jobe *et al*. (2016).

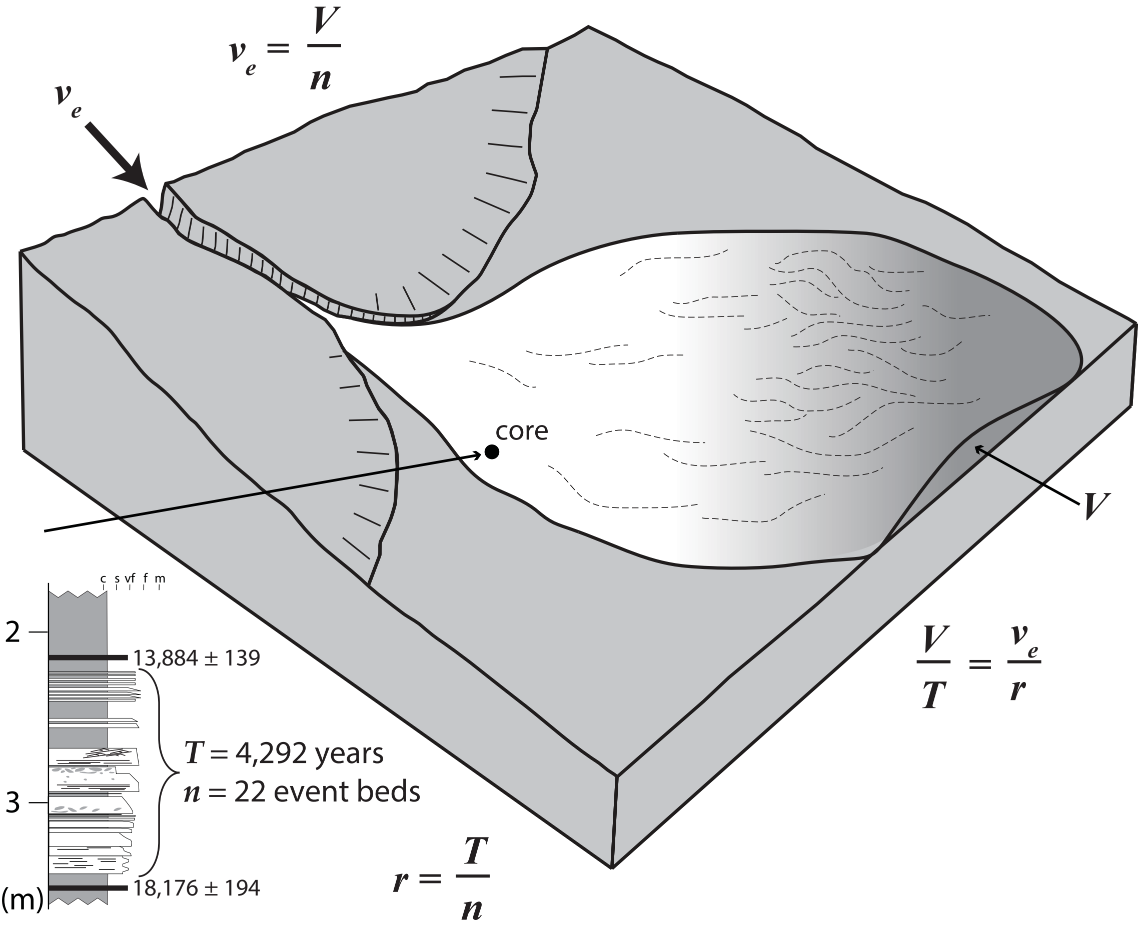

$v_e = \frac{V}{n}$
v_e
core
V
$\frac{V}{T} = \frac{v_e}{r}$
c s vf f m
2
3
(m)
13,884 ± 139
T = 4,292 years
n = 22 event beds
18,176 ± 194
$r = \frac{T}{n}$

Fig. 2. Map showing locations of late Quaternary submarine fan deposits analyzed in this study.

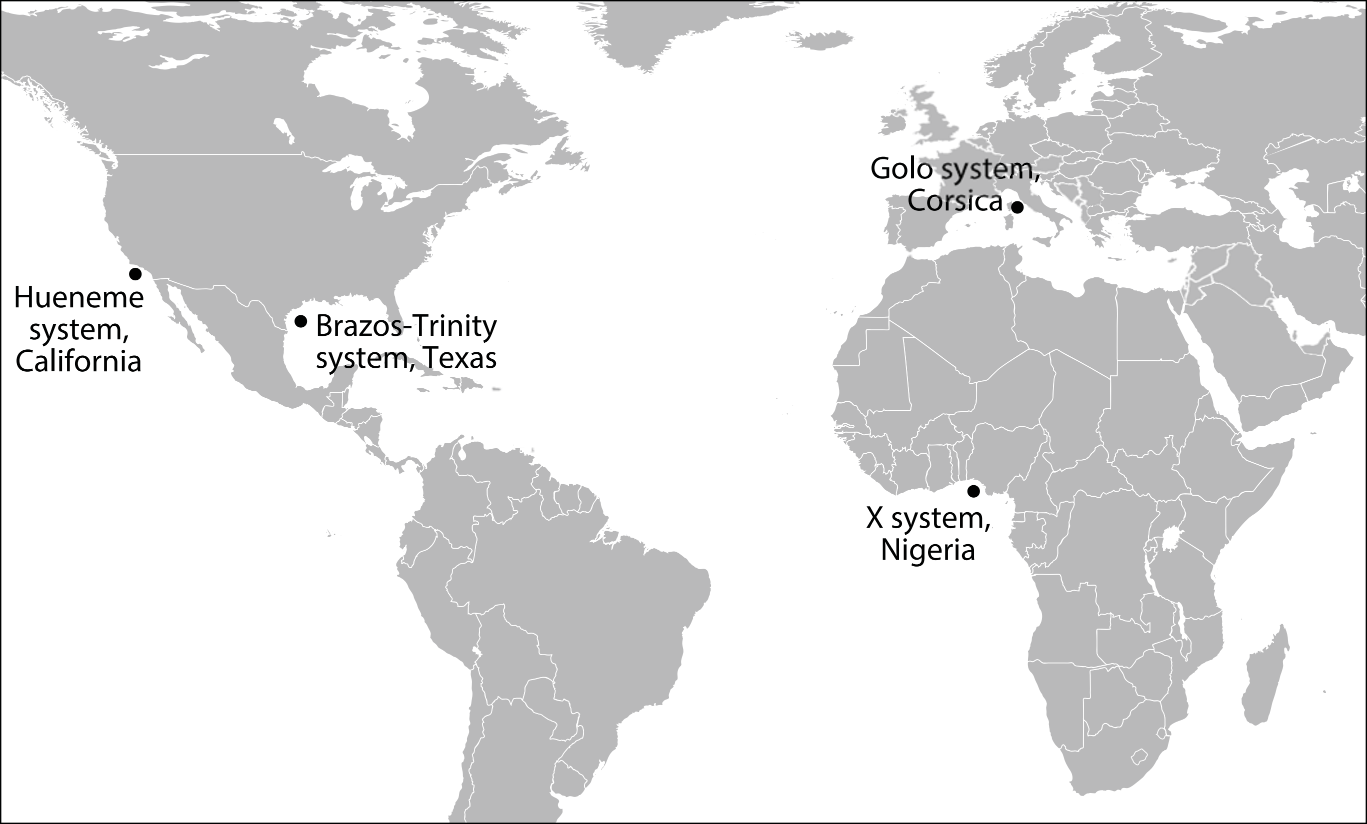
Golo system,
Corsica
Hueneme
system,
California
Brazos-Trinity
system, Texas
X system,
Nigeria

Fig. 3. Niger X fan seafloor depth map (10 m contours) with seismic amplitude (colour) and core locations (white circles). Two cores used in the calculation of turbidity current recurrence are shown at left and right. The black shaded region delineates the youngest sediment package of the Niger X fan. Figure modified after Jobe *et al*. (2016).

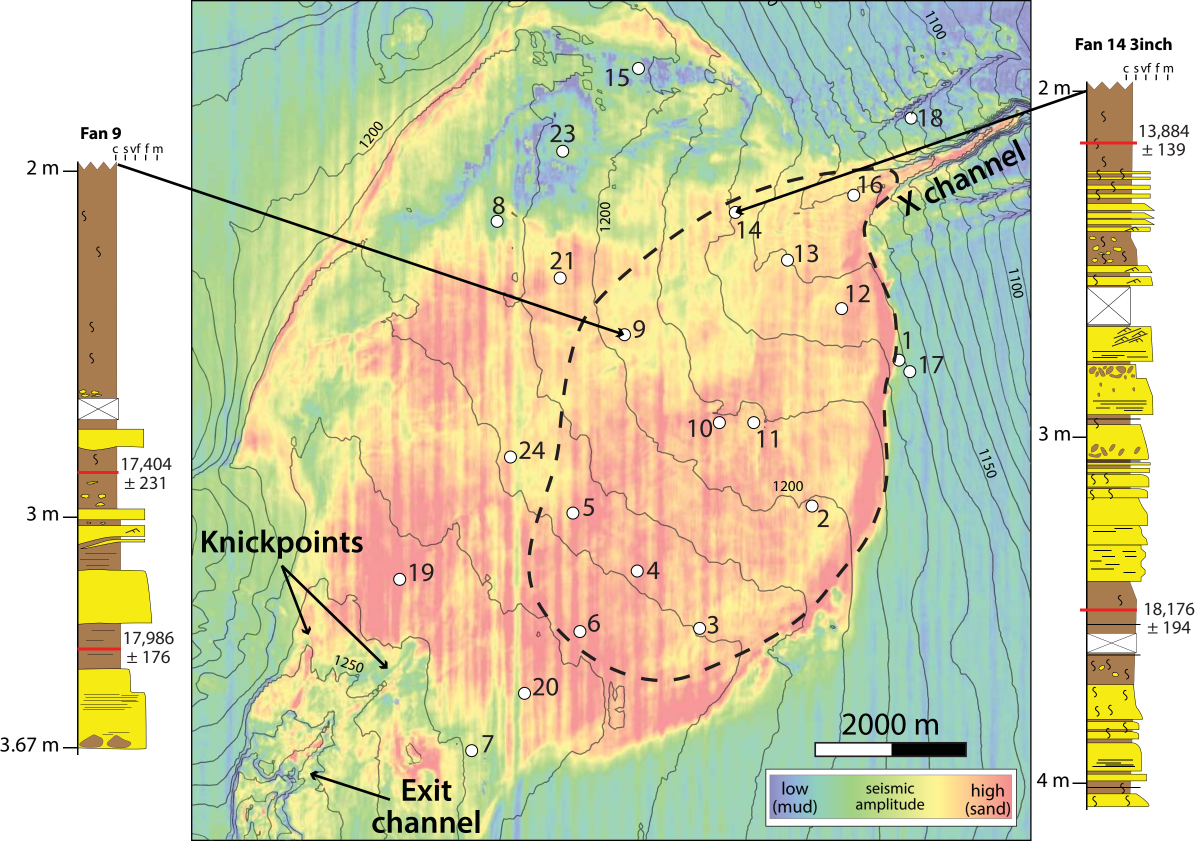

Fan 9
c s vf f m
2 m
17,404 ± 231
3 m
17,986 ± 176
3.67 m
Fan 14 3inch
c s vf f m
2 m
13,884 ± 139
3 m
18,176 ± 194
4 m
X channel
Knickpoints
Exit channel
1100
1150
1200
1250
2000 m
low (mud)
seismic amplitude
high (sand)
1
2
3
4
5
6
7
8
9
10
11
12
13
14
15
16
17
18
19
20
21
23
24

Fig. 4. Size-recurrence plot for formative turbidity currents of the Niger X fan using (A) uniform distributions of input values *V*, *T*, and *n* and (B) triangular distributions of input values *V*, *T*, and *n*. Grey dots are the 10,000 iterations, and the dashed line is the convex hull of the uniformly distributed data shown in part A. In (B), the black contour lines represent a 2D kernel density contour map of 90% of the data, and the cross is the data centroid.

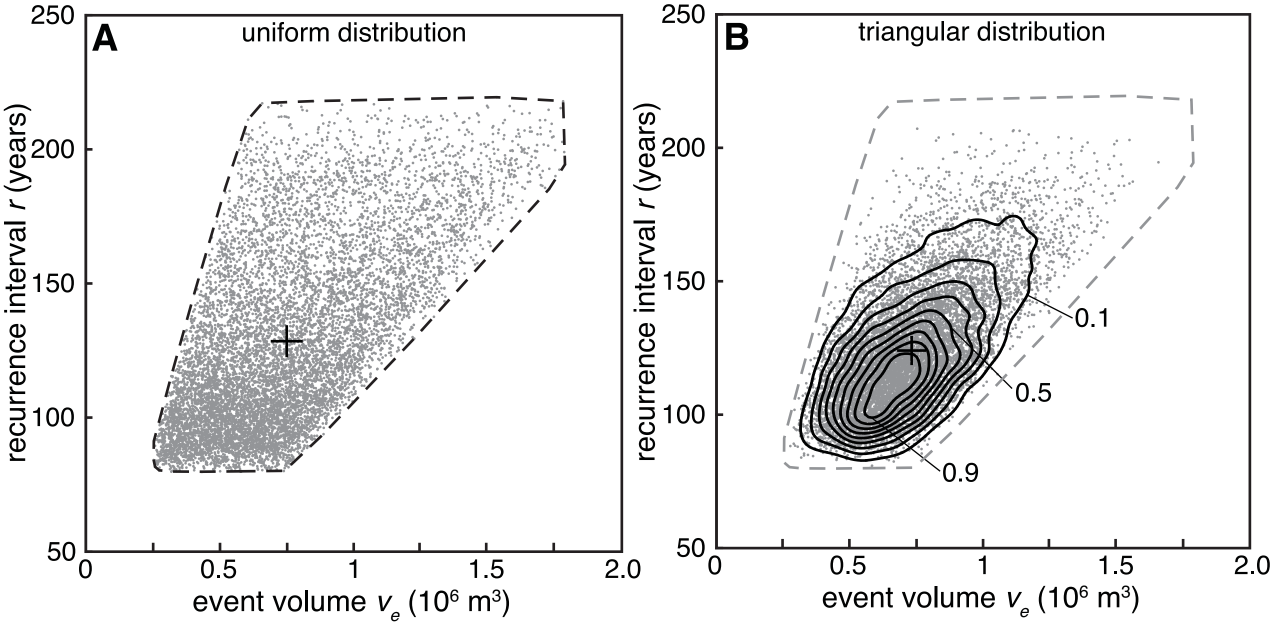

A
uniform distribution
B
triangular distribution
recurrence interval r (years)
event volume v_e (10^6 m^3)
250
200
150
100
50
0
0.5
1
1.5
2.0
0.1
0.5
0.9

Fig. 5. Parameter-space for event volume (v_e) and recurrence interval (r) of Quaternary submarine fan deposits. The convex hull is shown for each locale as calculated from uniformly distributed variables. Event volume varies over four orders of magnitude while recurrence interval only varies by one. Note that intraslope deposits tend to have lower event volumes than deposits of base-of-slope and ponded systems (see discussion in text).

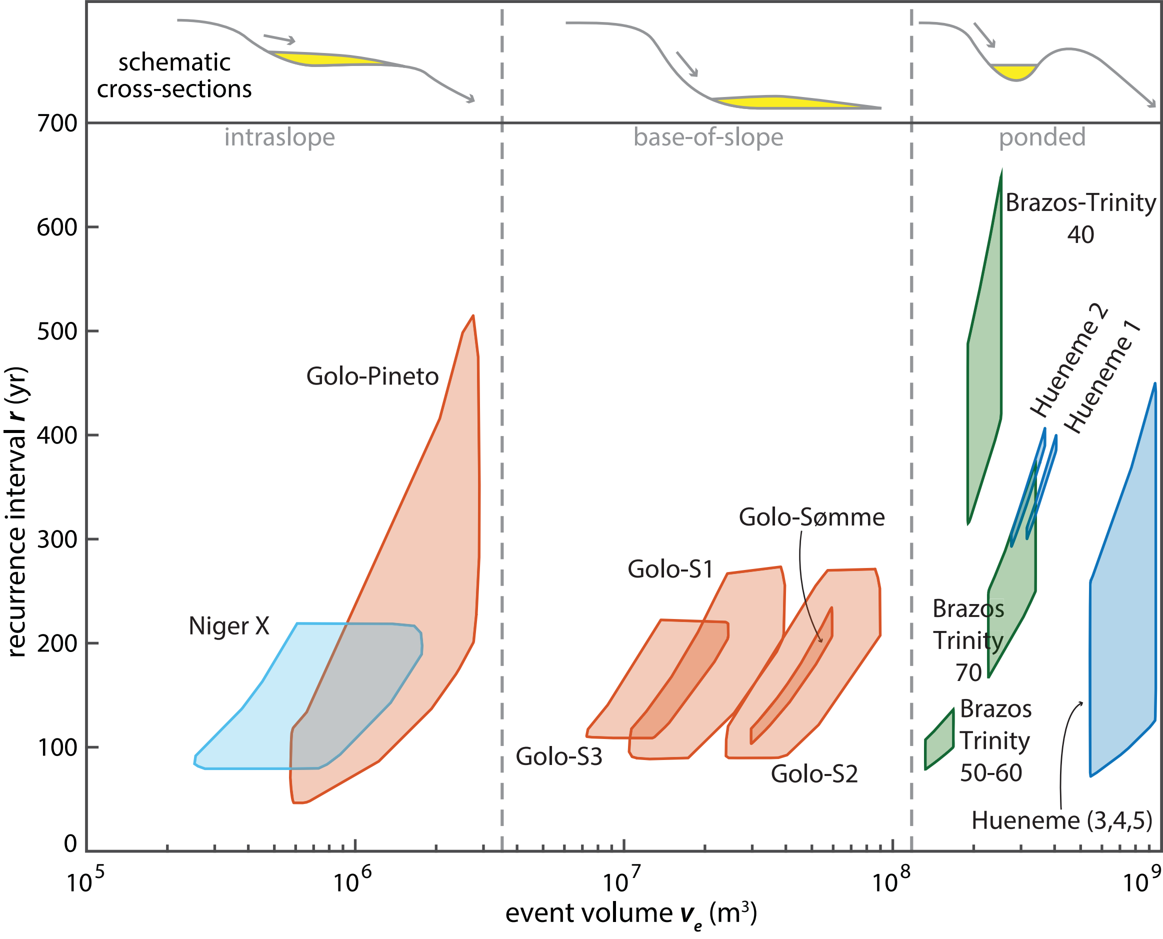

schematic
cross-sections
intraslope
base-of-slope
ponded
Golo-Pineto
Niger X
Golo-S1
Golo-S3
Golo-Sømme
Golo-S2
Brazos-Trinity
40
Hueneme 2
Hueneme 1
Brazos
Trinity
70
Brazos
Trinity
50-60
Hueneme (3,4,5)
recurrence interval r (yr)
event volume v_e (m^3)
0
100
200
300
400
500
600
700
10^5
10^6
10^7
10^8
10^9

Fig. 6. Cumulative distribution of the estimated total time of deposition (*T*) for submarine-fan deposits of the Permian Skoorsteenberg Formation, South Africa (nomenclature from Prélat *et al*., 2009). Vertical bars represent ranges of *T* for Late Quaternary Amazon and Zaire submarine-fan deposits.

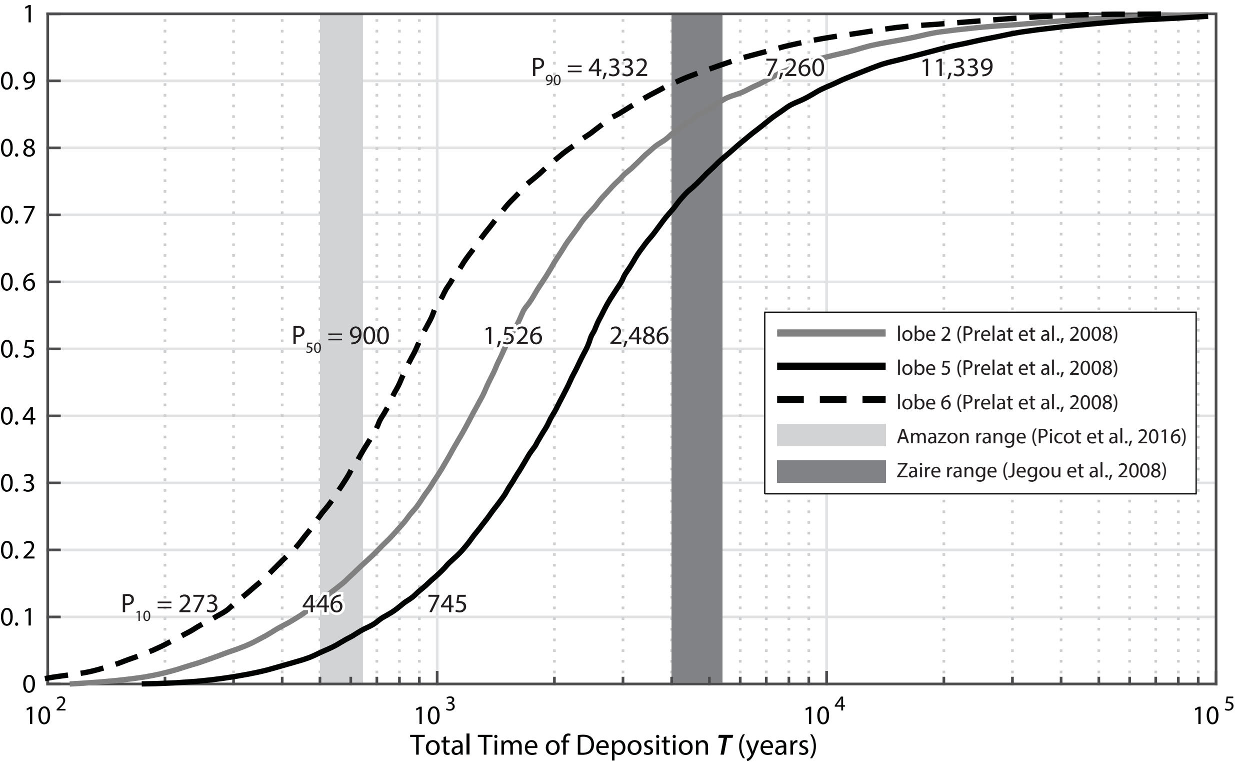

1
0.9
0.8
0.7
0.6
0.5
0.4
0.3
0.2
0.1
0
10^2
10^3
10^4
10^5
Total Time of Deposition T (years)
P_{90} = 4,332
7,260
11,339
P_{50} = 900
1,526
2,486
P_{10} = 273
446
745
lobe 2 (Prelat et al., 2008)
lobe 5 (Prelat et al., 2008)
lobe 6 (Prelat et al., 2008)
Amazon range (Picot et al., 2016)
Zaire range (Jegou et al., 2008)

Fig. 7. Scaling relationships between median event volume and catchment parameters (A) catchment area, (B) sediment yield, and (C) total sediment load. There is weak positive scaling between median event volume and catchment parameters (dashed arrows), particularly sediment yield. More systems need to be characterized to validate these scaling relationships. The Niger forms a consistent outlier, suggesting that the sediment partitioning (Allen, 1965) is inaccurate.

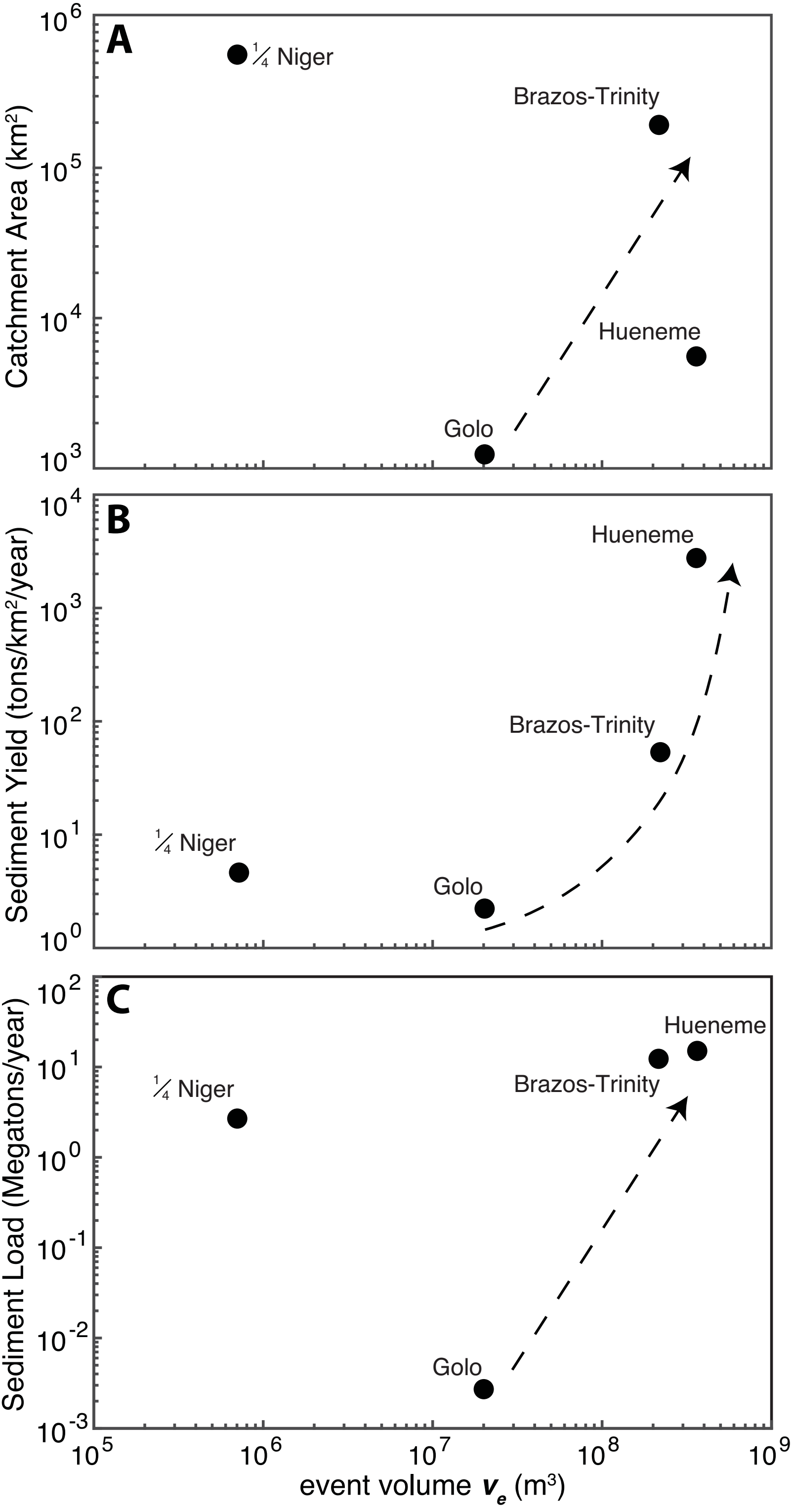

A
¼ Niger
Brazos-Trinity
Hueneme
Golo
Catchment Area (km²)
10^6
10^5
10^4
10^3
B
Hueneme
Brazos-Trinity
¼ Niger
Golo
Sediment Yield (tons/km²/year)
10^4
10^3
10^2
10^1
10^0
C
Hueneme
Brazos-Trinity
¼ Niger
Golo
Sediment Load (Megatons/year)
10^2
10^1
10^0
10^-1
10^-2
10^-3
10^5
10^6
10^7
10^8
10^9
event volume v_e (m³)

Fig. 8. Simplified parameter space for event volume and recurrence of turbidity currents across the submarine sediment routing system (inspired by Piper & Normark, 1983). Frequent, small volume flows begin in the canyon, but often do not reach the fan. Larger and less frequent flows build submarine fans, but generally do not reach the abyssal plain. Only very rare, very large flows reach the abyssal plain. The plot is overlain with a simplified submarine sediment routing system for visualization purposes. Note the overlap between the largest scales calculated by this study and that of abyssal plain turbidites, suggesting a continuum of flow properties between submarine fans and abyssal plains.

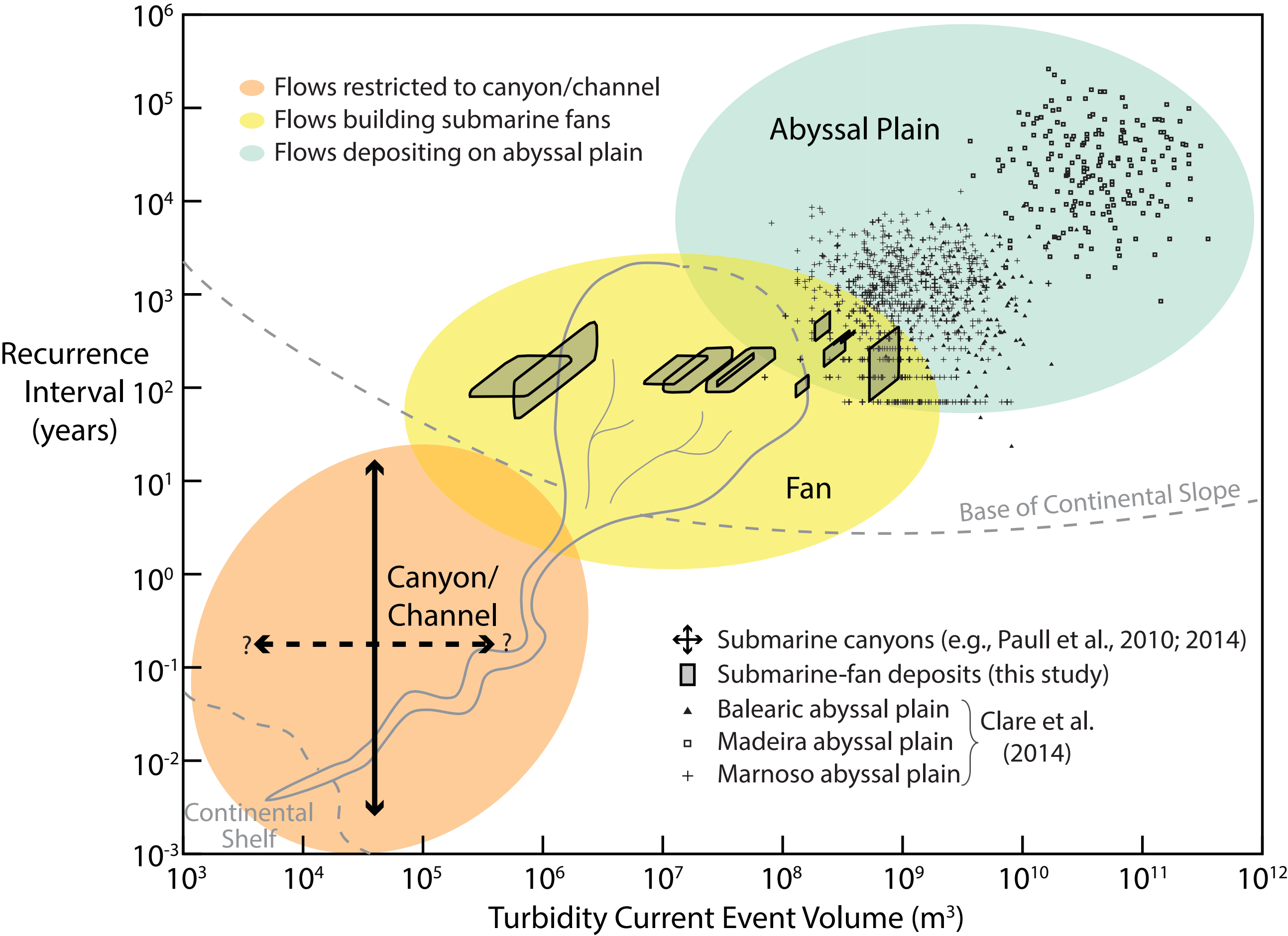

Flows restricted to canyon/channel
Flows building submarine fans
Flows depositing on abyssal plain
Abyssal Plain
Fan
Base of Continental Slope
Canyon/ Channel
Continental Shelf
Submarine canyons (e.g., Paull et al., 2010; 2014)
Submarine-fan deposits (this study)
Balearic abyssal plain
Madeira abyssal plain
Marnoso abyssal plain
Clare et al. (2014)
Recurrence Interval (years)
Turbidity Current Event Volume (m³)